Pergamon

International Journal of Machine Tools & Manufacture 43 (2003) 51–60

INTERNATIONAL JOURNAL OF
MACHINE TOOLS
& MANUFACTURE
DESIGN, RESEARCH AND APPLICATION

Sensing, modeling and control for laser-based additive manufacturing

Dongming Hu, Radovan Kovacevic *

Research Center for Advanced Manufacturing (RCAM), Southern Methodist University, 1500 International Parkway suite 100, Richardson, TX, 75081, USA

Received 25 June 2002; accepted 20 August 2002

Abstract

Laser-Based Additive Manufacturing (LBAM) is a promising manufacturing technology that can be widely applied to part preparation, surface modification, and Solid Freeform Fabrication (SFF). A large number of parameters govern the LBAM process. These parameters are sensitive to the environmental variations, and they also influence each other. This paper introduces the research work in RCAM on improving the performance of the LBAM process. Metal powder delivery real-time sensing and control is studied to achieve a controllable powder delivery for fabrication of functionally graded material. A closed-loop control system based on infrared image sensing is built for control of the heat input and size of the molten pool in the LBAM process. The closed-loop control results show a great improvement in the geometrical accuracy of the built features. A three-dimensional finite element model is also established to explore the thermal behavior of the molten pool in the closed-loop controlled LBAM process.

Keywords: Solid free form fabrication; Cladding; Image Sensing; Control; Powder delivery; Finite element modeling

1. Introduction

Building metal parts with good accuracy and mechanical properties for functional prototypes and products is one of the primary aims of Solid Freeform Fabrication (SFF). Several SFF methods have been developed to produce metal parts, such as 3D welding [1–3], micro casting [4], selective laser sintering (SLS) [5], and processes based on 3D laser cladding such as Laser Engineered Net Shaping (LENS) [6], Shape Deposit Manufacturing (SDM) [7], Directed Light Fabrication (DLF) [8], and Laser-Based Additive Manufacturing (LBAM) [9,10], and some other hybrid methods [11,12]. Compared to other SFF methods, processes based on 3D laser cladding have several advantages. In general, laser processing can produce relatively more accurate results with inducing much less heat. Because of the powder delivery feature in 3D laser cladding, no inert-gas protection chamber is required. So, a larger part can be produced, and a more complicated cladding path can be traced including four-dimensional and five-dimensional paths. By controlling the mass delivery rate of the metal powders from the different powder feeders, functionally graded materials can also be produced.

In 3D laser cladding, a large number of parameters govern the cladding process [13]; they are sensitive to the environment variations and influence each other. A first set of parameters is related to the equipment used: the laser, the focusing and beam shaping optics, the nozzle, the powder and gas delivery system, and the substrate on a moving stage. Another group of parameters is related to the interaction zone. There are two interaction zones. One zone is the space below the nozzle exit and above the substrate where the powder interacts with laser. The second zone is located at the substrate surface where a molten pool is formed by the heat of the laser, and the powder is projected into the molten pool to adhere to the substrate. Several research pursuits have been reported to improve the laser cladding process. Some of the research focuses on controlling the powder delivery system in order to achieve a stable or controllable powder delivery [14,15], or to study the powder

* Corresponding author. Tel.: +1 214 768 4865.
E-mail address: kovacevi@engr.smu.edu (R. Kovacevic).

0890-6955/03/$ - see front matter © 2002 Elsevier Science Ltd. All rights reserved.
PII: S0890-6955(02)00163-3

stream distribution and laser-powder interaction [16,17]. Others deal with the optimization of the laser cladding process with closed-loop control, using a CCD camera [18–21] or a phototransistor [22] as the sensing device. In order to obtain a robust and controllable laser deposition process, modeling of the laser deposition is required to understand the thermal behavior of the molten pool. There are numerous research attempts reported on the numerical modeling of the laser material processing such as laser welding and laser cladding [23–26].

The controllable powder delivery can greatly improve the performance of 3D laser cladding. It provides the feasibility to build a functionally graded material or alloy. The key component for achieving powder delivery control is a real-time powder delivery rate sensing and control unit. Most commercial powder delivery systems use continuous weight measuring for feedback. The weight measuring method has a large time delay to achieve a desired stable powder delivery rate. Some research work provides different methods for real-time powder delivery rate sensing, such as applying an optoelectronic sensor [14], and increasing the weight sampling rate by modifying the structure of the powder feeder [15], but those works are specific to the particular powder feeders and focus on the applications of two-dimensional surface cladding. A study on the system for controlling of the multiple metal/ceramics powder feeding systems is also required.

The sensing of the molten pool to control 3D laser cladding is of great importance. A few attempts on sensing the molten pool have been reported that utilize infrared image as a sensing method acquired by a CCD camera [18–21] or a phototransistor [22]. However, the CCD camera or the phototransistor is usually installed from one side of the nozzle. The distance between the nozzle and the substrate is very small (~5 mm); so, the field of view is drastically limited. The images are deformed due to the large angle between the optical central line of the camera and laser-nozzle setup. Also, the images acquired from an asymmetrically installed camera vary because of the lack of omni-directionality. A coaxial installation of the camera has big advantages for molten pool sensing [21].

Single-bead wall building is a good study case for modeling the thermal behavior of the molten pool in the 3D laser cladding because it is a basic geometrical feature that the 3D laser cladding is capable of building, and experiences critical processing conditions. However, only one research work is reported on building the single-bead wall by the 3D laser cladding process [27,28] while the model is limited to two-dimensions without considering the influence of the thickness of the wall. There are some difficulties in establishing a three-dimensional numerical model to simulate the process of building a single-bead wall. The thickness of the wall is identical to the width of the molten pool, which is determined by the processing parameters (laser power, traverse velocity, etc) and heat balance conditions. The width of the molten pool varies in the open-loop laser deposition process according to the processing conditions in a complex relationship. It is impractical to build a three-dimensional numerical model with a constant wall thickness and a predefined laser power for the 3D laser cladding processes under different processing conditions.

In this paper, research efforts for developing Laser-Based Additive Manufacturing (LBAM) are introduced. Sensing and control technologies are applied to improve the overall performance of the LBAM process for Solid Freeform Fabrication. Real-time sensing and control of the metal powder delivery rate is studied to achieve a controllable powder delivery for the fabrication of functionally graded materials. A closed-loop control system is developed for heat input control in the LBAM process, based on the infrared image sensing. The experimental results of closed-loop controlled LBAM show a great improvement in the geometrical accuracy of the part being built. A three-dimensional finite element model is also established to explore the thermal behavior of the molten pool in closed-loop controlled LBAM process. The complexity of the numerical modeling caused by the variation of the molten pool can be regulated by the closed-loop controlled LBAM process. A constant width of the molten pool can be achieved in the closed-loop controlled LBAM process, and a single-bead wall with a uniform thickness can be built. It enables the establishment of a simpler but more realistic numerical model for single-bead wall building in which a constant wall thickness can be applied. Results from the finite element thermal analysis have provided guidance for process parameter selection in LBAM, and develop a base for further residual stress analysis.

2. Sensing and control of powder delivery

The controllable powder delivery can greatly improve the performance of 3D laser cladding. It provides the feasibility to build a functionally graded material or alloy. The key technology to implement powder delivery control is the real-time sensing of the metal powder delivery. Most of LBAM systems are equipped with commercial powder delivery systems designed for a plasma spray process in which a higher powder delivery rate is desired. The powder feeder is equipped with an electronic scale to continuously measure the weight of the metal powder inside the hopper, and it uses the change of weight as a feedback to control the powder delivery rate. Due to the low sampling frequency of the feedback, a steady delivery rate can only be realized if the delivery rate is averaged in a long period of time after the feed screw reaches a stable rotational speed. In

a smaller time scale, fluctuations in the powder delivery can be observed.

An optoelectronic sensor is developed to sense the metal powder delivery rate in real-time. The sensor consists of a laser diode, a photo diode, and a glass window. The components are installed in such a way that the laser beam emitted from the laser diode passes through the powder stream flowing inside the glass chamber and is received by the photo diode (Fig. 1 (a)). The carrier gas and the metal powder are mixed well so the powder particles distribute uniformly in the carrier gas. Because of the diffusion, absorption, and reflection of the powder particles to the laser beam, the laser energy received by the photo diode decreases if the powder delivery rate increases, which means there is higher percentage of powder particles in the carrier gas. The laser diode emits a red light with a wavelength of 600–710 nm and a power less than 500 mW. The photo diode is characterized with a good linearity between the illumination energy received by the diode and the output current that is converted later to a voltage signal through a current signal pick-up circuit. Fig. 1 (b) shows the setup of the metal powder delivery rate sensor.

A group of experiments are set up to test and calibrate the sensor. By setting the feed screw of the powder feeder at different rotational speeds, a series of powder delivery rates can be obtained. The feed screw runs at the preset rotational speed for about 2 min before any measurement is taken to ensure that a static delivery status has been reached. The averaged powder delivery rate is then calibrated by measuring the time period and the weight of the powder delivered during that time period. The corresponding sensing signal from the sensor is also acquired at 10 Hz by a data acquisition card installed on a PC. The averaged sensor output voltage presented in Fig. 2 exhibits a near linear relationship to the averaged powder delivery rate in the range of 3–22 g/min. In most of LBAM applications, the powder feed rate is below 15 g/min. In such a range, the sensor provides a good sensing and feedback feature for the further control of the metal powder delivery rate. The sensing signal of the powder delivery rate from the developed sensor is utilized as a feedback to control the rotational

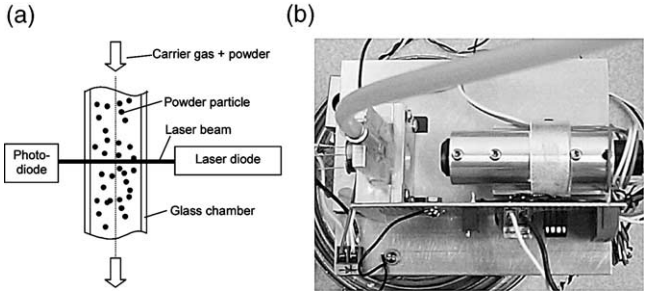

Fig. 1. Powder delivery rate sensor. (a) Schematic of the powder delivery rate sensor. (b) Setup of the powder delivery rate sensor.

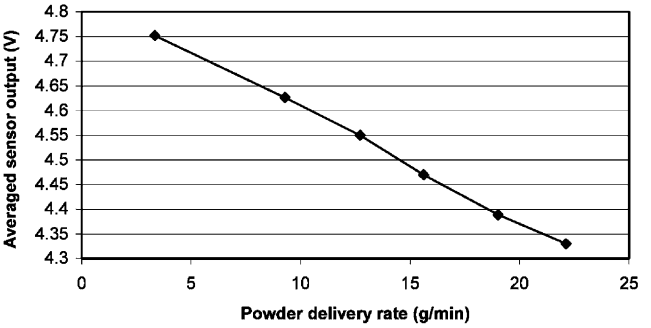

Fig. 2. Output performance of the powder delivery rate sensor.

speed of the feed screw. The real time sensing at a higher sampling frequency provides the powder feeder with a feasibility of a more uniform and controllable powder delivery. A precise delivery of the functionally graded material can also be implemented based on the powder delivery sensing and simultaneously controlling multi powder feeders.

A new embedded powder controller is developed. As a standalone controller, the powder feeder controller acquires the weight of the whole powder feeder from the electronic weight scale through the RS232 connection, and reads the powder delivery rate from the optoelectronic sensor through an A/D converter. The motor speed is controlled based on the feedback from the weight scale and the optoelectronic sensor; so, a stable powder delivery rate can be reached. Several controllers can be linked to the central control PC computer through Ethernet or RS485 serial connections to form a control system for controlling multiple powder feeding systems. Each controller controls one powder feeder. A system control software supports TCP/IP, and serial port communication protocols are running on the central PC. Sending the commands through Ethernet or RS485 serial connections, the desired delivery rate of each kind of powder is controlled by the central PC in real time. Up to four powder feeders can be controlled simultaneously by the central PC. Functionally graded material can be fabricated by synchronizing the motion, laser operating parameters, and powder delivery rates according to the design of the material. Fig. 3 shows the schematic and real setup of multiple powder feeding systems.

3. Control the molten pool based on infrared image sensing

A coaxial infrared image sensing setup with respect to the metal powder delivery nozzle has been developed. As shown in Fig. 4 (a), the laser head consists of a partial reflective mirror and lens set. The Nd: YAG laser beam inducted by the optical fiber is reflected from the partial reflective mirror, and it is focused on the substrate by the set of lenses arranged in the laser head. The optical

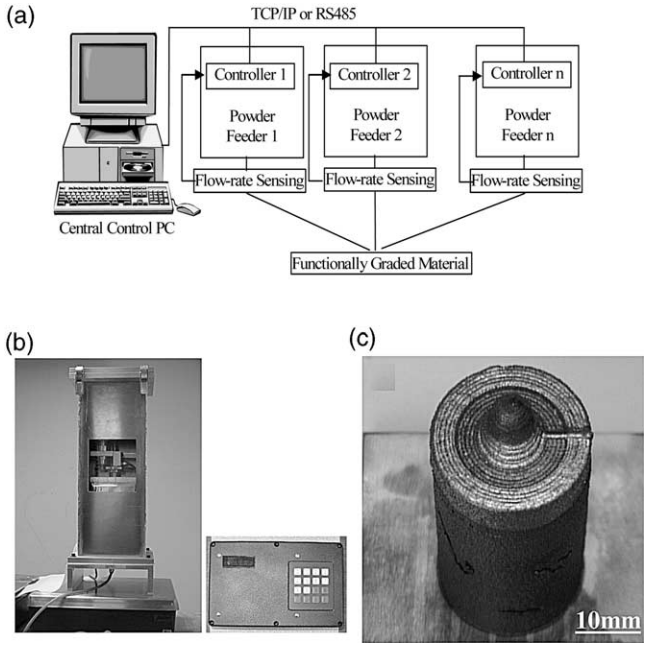

Fig. 3. Multiple powder feeding system. (a) Schematic of multiple powder feeding system. (b) Newly designed powder feeder and controller. (c) Part built by multiple powder feeding systems.

part of the laser head forms another optical path for the observation of the laser processing. A high frame-rate (up to 800 frames/s) camera installed at the top of the laser head takes gray images with a 128×128 resolution. The radiation from the molten pool produced by the laser beam passes through the partial reflective mirror and forms an image on the CCD chip of the camera. A Nd: YAG laser blocker (1.06 μm) is utilized to protect the camera from laser damage. An iris is used to adjust the intensity of the radiation received by the camera to prevent over exposure. In order to get the infrared image of the molten pool to reduce the high intensity light from the molten pool and eliminate the image noise from the metal powder, an infrared filter is selected ($>$ 700 nm) and installed between the iris and the camera. During the LBAM process, the camera acquires images of the build up process at a constant frame rate. Images are transferred to a frame grabber installed on a PC that carries out the image processing and control process. The real setup of the infrared image acquisition system is shown in Fig. 4 (b).

Fig. 5 (a) provides the original infrared image acquired by the coaxially installed camera. Because the observation is directly from the top of the molten pool, a full field of view of the molten pool can be acquired without any blocking. With a right combination of the Nd: YAG filter and the IR filter as well as a right adjustment of the iris, a clear image of the molten pool and the surrounding thermal area can be obtained without the noise from the metal powder. The radiation wavelength received by the camera is between 0.7 and 1.06 μm. The

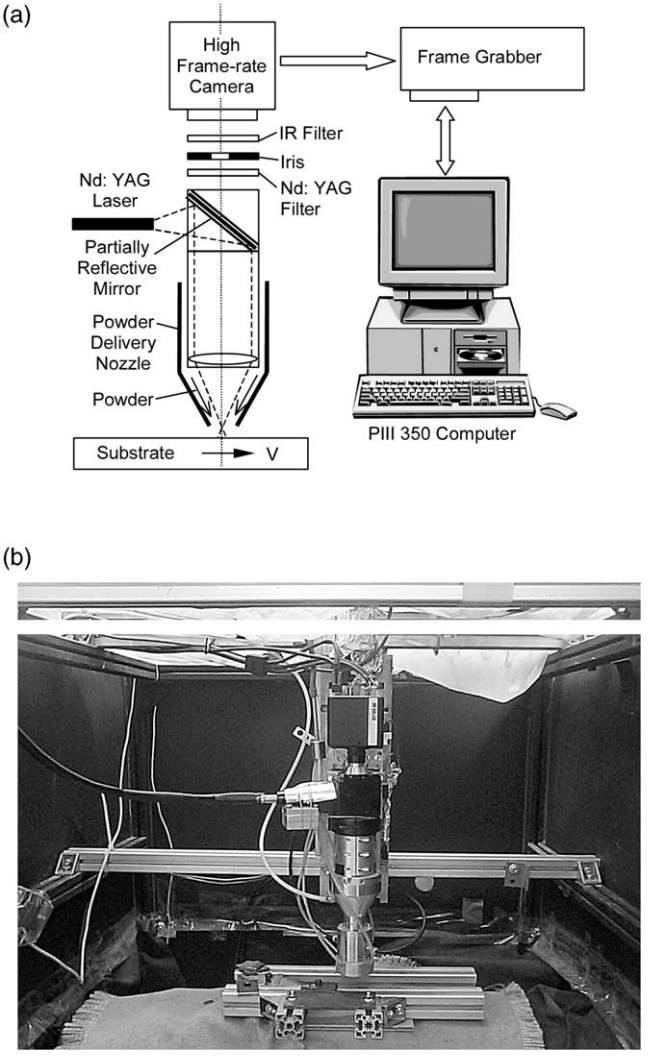

Fig. 4. Infrared image acquisition system. (a) Schematic. (b) Experimental setup.

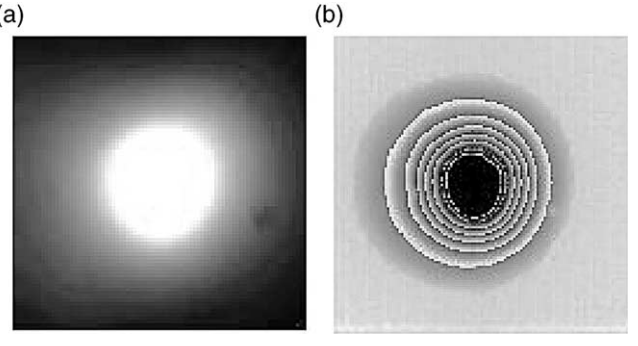

Fig. 5. Infrared image acquired. (a) Original infrared image. (b) Grey level isotherms.

infrared images acquired reflect the temperature distribution in the molten pool and surrounding area.

Fig. 5 (b) shows the grey level isotherms of the infrared image that indicate the temperature distribution in

the molten pool and surrounding area. In order to determine the grey level value corresponding to the liquid-solid transient edge of the molten pool in the infrared image, an ultra-high shutter speed camera with a pulsed nitrogen laser is installed on the side of the laser head. The powder delivery nozzle is removed to provide sufficient installation space and to ensure an undisturbed view under the Nd: YAG laser head for the high shutter speed camera. Calibrations to the physical dimensions for both of the cameras are accomplished first by taking images of a referenced target. Then, the ordinary and infrared images of the molten pool are acquired simultaneously by synchronizing the two cameras while the Nd: YAG laser is projected on the moving substrate. The pulsating nitrogen laser emits light with the wavelength of 337 nm to provide an illumination in the laser processing area for the high shutter speed camera. A notch filter of 337 nm is also installed inside the high-speed shutter camera that allows light to pass with a wavelength only around 337 nm. The pulsating illumination synchronized with the high-speed shutter on the camera suppresses the intensive light from the molten pool, and ensures the successful acquisition of clear images of the molten pool. The ordinary images acquired from the high-speed shutter camera are processed with a Canny edge detector to find the edge of the molten pool [19]. By mapping the position of the edge of the molten pool from the ordinary image to the corresponding infrared image through a coordinate transformation, it is determined that a grey level of 70 represents with enough accuracy the transition between the molten pool and the surrounding solid.

The LBAM system comprises four subsystems: a 1-kW Nd:YAG laser source, a metal powder delivery system, a 3-axis positioning system, and an infrared image acquisition system. The 3D metal part is produced layer by layer by synchronizing the X-Y-Z motion, the Nd:YAG laser, and the injection of metal powder. The infrared image acquisition system takes the images of the molten pool in real time and calculates the dimensions of its area. It compares the recorded information to the preset value and creates a feedback control value to modify the output of laser source. In this way, a stable molten pool or its corresponding thermal filed area with desired dimensions is obtained, and thus it is possible to produce stable and repetitive layers if a stable powder flow rate is ensured. A simple PID controller is applied to build the closed-loop control system. Because of the existence of some 'lag' (less than 100 ms) in laser-computer parallel port communication, a feed forward compensation is also introduced for control of the molten pool area.

Two single-bead walls are built respectively by an open loop and closed-loop controlled LBAM process to compare the processing results. The nozzle moves along the positive direction of the X axis first to build one layer, moves up for a small increment along the Z axis after the layer is built up, and then moves back along the negative direction of the X axis for the next layer's deposition. The threshold for counting the area of the molten pool in the number of pixels is set to 70 indicating the grey level of the edge of the molten pool. The images are recorded continuously with an image-processing rate of 15 frames/sec during the wall building. The substrate material utilized in the experiments is mild steel, and the metal powder is an H13 tool steel powder with a $+100/-325$ mesh size. The powder delivery rate is kept constant.

A 50-layered single-bead wall is built first by the uncontrolled LBAM process. The processing parameters utilized in the experiment are a 5-mm/s scanning speed, a 4 g/min powder delivery rate, a 0.25-mm Z-height increment, and a 420-W constant laser power. Fig. 6 shows the signal of the molten pool area valued in the number of pixels greater than the preset threshold. The number of frames can be regarded as the processing time due to the constant image acquisition rate. Each pulse in Fig. 6 represents one cladded layer. Fig. 6 (a) displays the signal of the whole process from which the overall variation trend can be observed. The zoomed-in signal for two selected layers is given in Fig. 6 (b). This signal provides the information for the variation of the molten pool area along one cladded layer. The finished part is shown in Fig. 6 (c).

The uncontrolled LBAM is affected by the changes in the heat loss. At the beginning of the wall building due to the large heat conduction of the substrate, the created beads are narrower. As the wall grows up, there is less heat conduction along the built wall, and the bead becomes wider until it reaches a new equilibrium value. From the cross-section of the wall shown in Fig. 6 (c), it can be seen that the root of the wall is narrower than the upper part of the wall. It can also be observed from Fig. 6 (a), that the pixel number of the molten pool area is 4000 for the first layer, and it gradually increases to around 10,000. The molten pool area also changes along one cladded bead. The two ends of the bead have less time to cool down than the middle segment of the bead. So, without laser power control, the two ends of the bead can reach a higher temperature reflected by the peak of molten pool area shown in Fig. 6 (b). The higher temperature results in more powder melting and cladding, and causes the higher build up at both ends of the wall that can be seen in Fig. 6 (c). It is a very common situation in 3D laser cladding that heat loss varies according to the part's geometric features and scanning paths. So without a closed-loop control, LBAM cannot provide a uniform geometry of the built layers.

A closed-loop controlled LBAM is carried out using the same processing parameters to build a 60-layered single-bead wall in order to test the performance of the developed control system. The reference value of the molten pool area is set to 5000. The molten pool area,

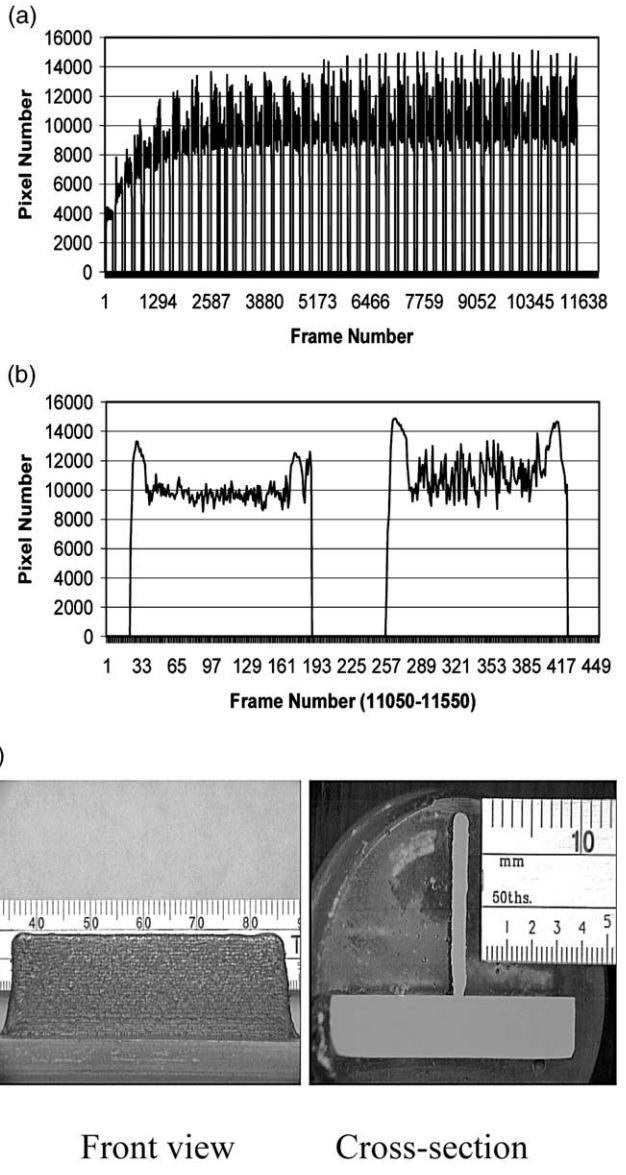

Fig. 6. Experimental results by open-loop LBAM. (a) Molten pool area signal of fifty layers. (b) Molten pool area signal of two layers. (c) Single-bead wall built.

laser power control signals and the built part are presented in Fig. 7. The closed-loop controlled LBAM system shows a very good performance. As shown in Fig. 7 (a), the molten pool area is controlled around the reference value during the wall building process. The laser power is decreased from 80 to about 60% to keep the molten pool area constant (Fig. 7 (b)). In one single-bead cladding process, the increase of the molten pool area at the both ends of the bead indicates the higher temperature is reduced due to the action of the closed-loop control. The built wall shown in Fig. 7 (d) is characterized by a uniform thickness. There are no build-ups at the end of the wall. From the cross-section of the wall, it can be seen that the width of the wall is constant.

To further compare the processing results, single-bead

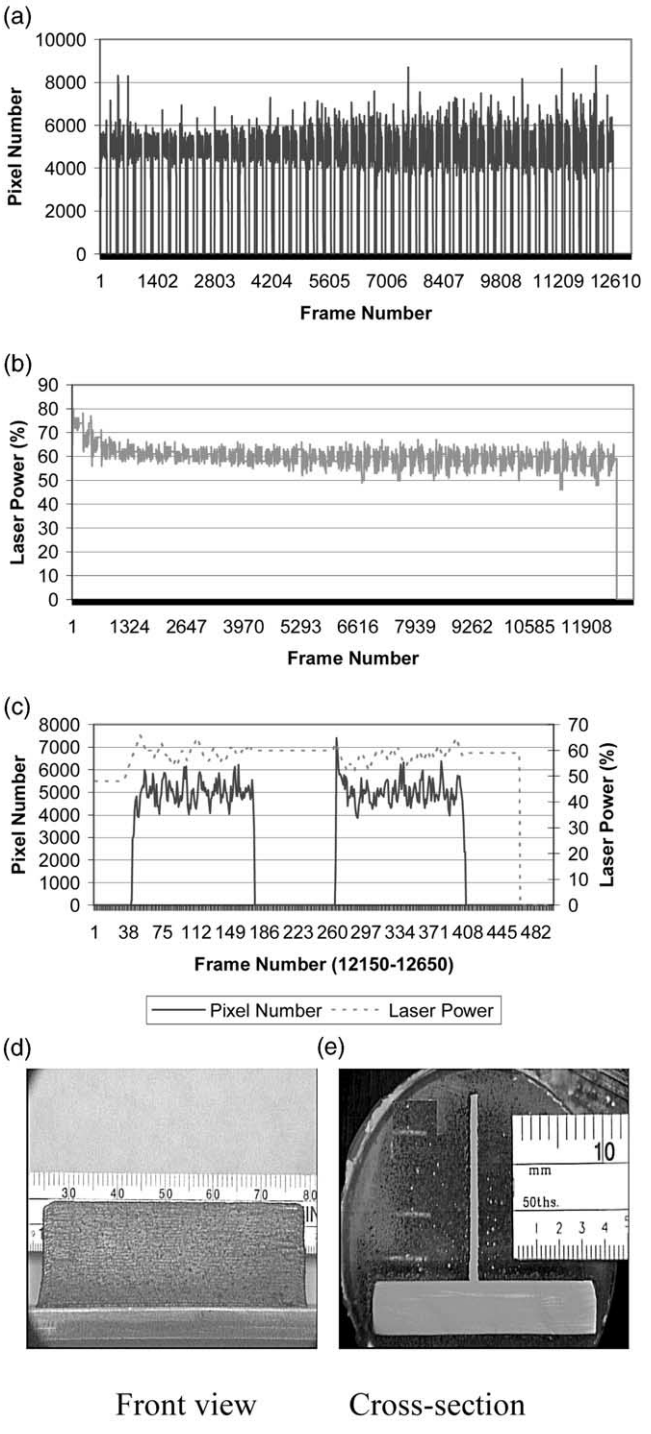

Fig. 7. Experimental results by closed-loop controlled LBAM. (a) Molten pool area signal of sixty layers. (b) Laser power control signal for sixty layers. (c) Molten pool area and laser control signal for two layers. (d) Single-bead wall built.

walls are built under the following three processing conditions [9]. The first type of sample is built with no pre-heating to the substrate and no closed-loop control of the heat input. The second type of sample is built with pre-heating but no control, and the third type of wall is

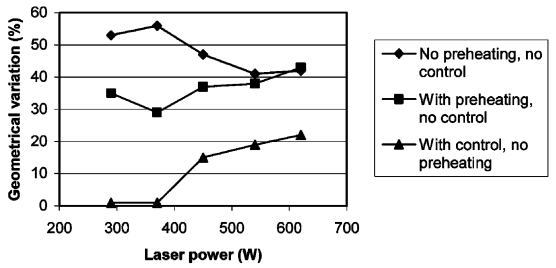

Fig. 8. Comparison of geometrical variations in laser cladding.

built utilizing the closed-loop control function without preheating. The average width of the wall W_a is calculated by averaging the ten width measurements taken at ten evenly spaced heights from the substrate surface. W_{min} means the minimum width of the wall that normally corresponds to the root of the wall. A geometrical variation coefficient η is introduced to express the width variation of each wall sample that is calculated by the following formula:

$$\eta = \left| \frac{W_{\mathrm{d}} - W_{\mathrm{min}}}{W_{\mathrm{a}}} \right| \times 100\% \tag{1}$$

The geometrical change of the walls as a function of laser power is shown in Fig. 8. When no heat input control is applied, a preheating procedure contributes to the improvement of the geometrical accuracy of the wall, especially when the laser power is less than 500 W. With an increase of laser power, the influence of preheating becomes less important because a higher laser power can compensate the heat loss for the different thermal conditions. It can also be observed that under all laser power levels, the geometrical variation of the cross sections of the built walls with a heat input control is much lower than those without control. When the laser power is below 400 W, there is nearly no width variation along the wall height if a control function is applied. Even at higher laser power levels, the geometrical accuracy gradually goes down but still is still much higher than a wall built without a control function. More complex 3D parts are built by the closed-loop controlled LBAM process (Fig. 9). The parts show sufficient geometrical accuracies.

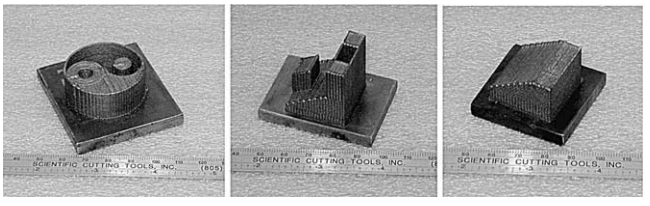

Fig. 9. Samples built by closed-loop controlled LBAM process.

4. Finite element modeling of thermal behavior of molten pool

The complexity in numerical modeling cased by the variation of the molten pool can be regulated by the closed-loop controlled LBAM process. A constant width of the molten pool can be achieved in the LBAM process, and a single-bead wall with a uniform thickness can be built. The closed-loop controlled LBAM enables the establishment of a simpler but more realistic numerical model for single-bead wall building in which a constant wall thickness can be applied. A three-dimensional finite element model is developed using ANSYS to study the thermal behavior of the molten pool in building a single-bead wall via a closed-loop controlled LBAM process. The building process of one layer on top of the single-bead wall with a certain height h is simulated. The model of the single-bead wall has a constant thickness w. The input laser power is varied to ensure the width of the molten pool is identical to the thickness of the wall during the deposition process. The temperature distribution, geometrical feature of the molten pool, and cooling rate for different process conditions are investigated.

A numerical simulation is carried out to analyze the thermal behavior of the closed-loop controlled LBAM process. Fig. 10 shows the results of the simulation of one layer building that applies the following processing parameters: $v = 5$ mm/s, $w = 1$ mm, $h = 10$ mm, and $L = 40$ mm. The laser power parameter in Fig. 10 is proportional to the laser output power and is adjusted according to the shape of the molten pool. By varying the laser power, the maximum temperature on the wall edge is controlled around the melting point; so, the width of the molten pool identical to the width of the wall can be obtained. In the simulation, the maximum temperature on the wall edge is controlled in the range of 1785–1788 K. The shape of the molten pool and fusion depth are kept constant during the layer building by closed-loop controlled LBAM; although, the cooling condition varies due to the geometrical feature of the single-bead wall. In the simulation of building one layer, the cooling condition changes at the two ends of the wall. During the wall building process, the cooling condition varies with the height of the wall, substrate temperature, etc.

The average temperature in the laser-material interaction zone contributes to the thermal residual stresses. The cooling rate at the edge of the molten pool determines the microstructure. The fusion depth determines the depth of the dilution of one layer into the other. These concerned thermal behaviors of the molten pool are not easily determined experimentally but can be analyzed from the numerical simulation result. Fig. 11 (a) gives the average temperature in the processing zone (the molten pool and the surrounding area) and the average cooling rate on the edge of the molten pool from the

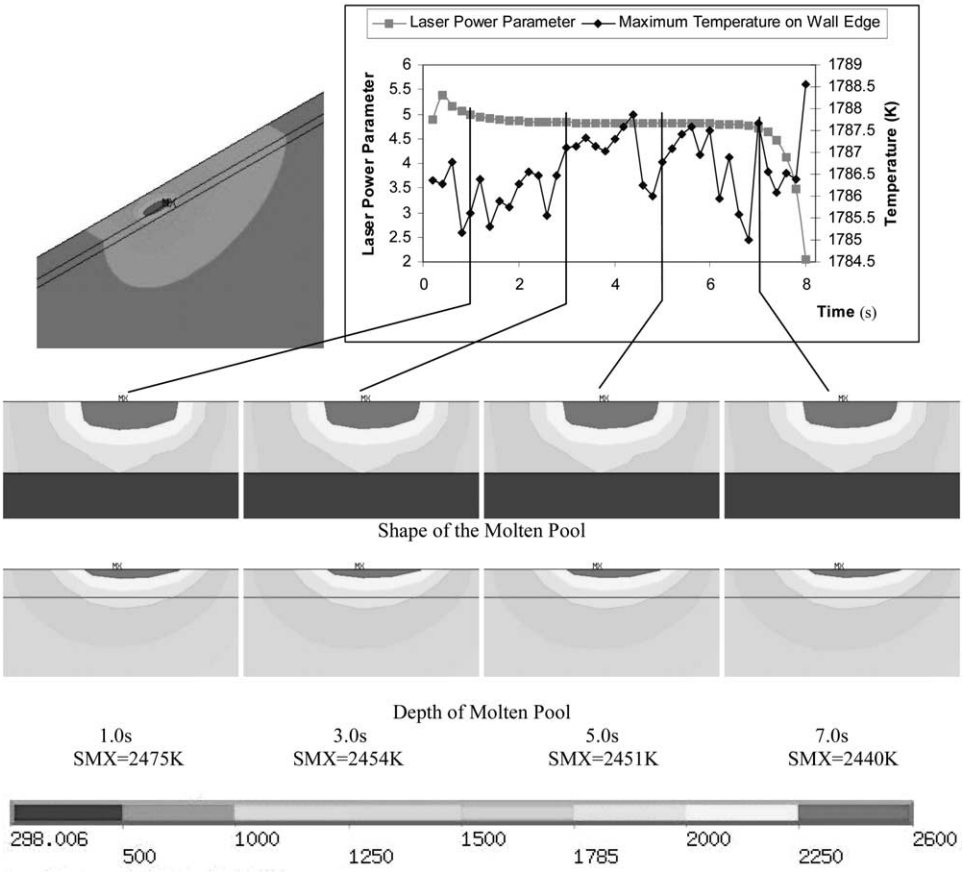

Fig. 10. Simulation results for building one layer by closed-loop controlled LBAM.

same simulation result shown in Fig. 10. Although the cooling rate on the edge of the molten pool is much less than the cooling rate of solidification because the time interval is 0.2 s for each calculation, it reflects the qualitative trends of the cooling rate of solidification. The corresponding results from the simulation of an uncontrolled LBAM is also presented for comparison. The curves in Fig. 11 (a) show that a controlled LBAM achieves a more stable average temperature, which predicts even thermal residual stresses. The cooling rate is heavily influenced by the cooling conditions (in this case, the heat conduction in different positions). However, it can be regulated in a smaller range by controlling the heat input. Such an improvement results in more uniform microstructures.

Different combinations of the traverse velocity and width of the wall are applied in different simulations to investigate the influences brought about by the processing parameters. Fig. 11 provides a comparison of simulated and experimental results. It can be seen from the figure that as the width of the molten pool increases, the depth and length of the molten pool, and average temperature in the processing zone increase. For the process in which the width of the molten pool is kept constant, the traverse velocity contributes little to the variations of the geometrical features of the molten pool and the average temperature in the processing zone. The average cooling rate is influenced significantly by the traverse velocity. A roughly proportional relationship can be found between the traverse velocity and the average cooling rate. Although the average cooling rate decreases as the width of the molten pool increases, the variation is only considerable when the traverse velocity is high. It can be concluded that the fusion depth and the average temperature in the processing zone can be regulated effectively by controlling the width of the molten pool; whereas, the desired average cooling rate can be reached by changing the traverse velocity. Whenever a constant width of the molten pool is achieved, constant geometrical features of the molten pool are obtained; so, controlling the area of the molten pool takes the same effort as controlling the width of the molten pool.

5. Conclusions

An optoelectronic sensor is developed that is capable of sensing the powder delivery rate in real time at a high sampling frequency. The sensing signal has a good lin-

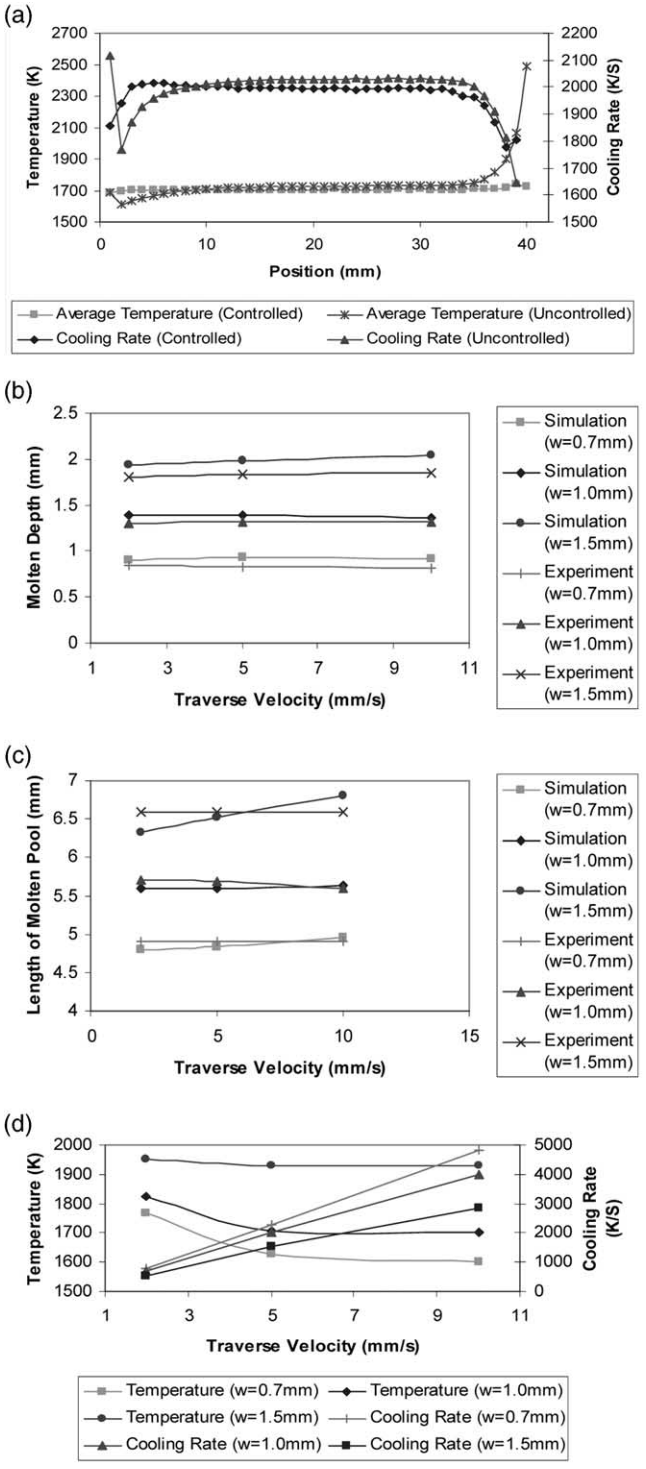

Fig. 11. Simulation results in building a single-bean wall. (a) Average temperature and cooling rate in one building layer. (b) Depth of molten pool under different processing conditions. (c) Length of the molten pool under different processing conditions. (d) Average temperature and cooling rate under different processing conditions.

earity with the averaged powder delivery rate. The successfully developed powder delivery sensor is a base for further study on the powder delivery control that ultimately will lead towards a precise functionally graded material delivery. Infrared image sensing is an efficient sensing method to improve the performance of LBAM. The coaxial installation of the camera ensures that the clear infrared images of the molten pool and its surrounding thermal area can be acquired easily with a short nozzle-substrate distance and different scanning directions. The infrared image can eliminate the image noise caused by the metal powder and is easy to be processed in real-time. The image reflects the temperature information that is a significant parameter affecting the cladding result. The closed-loop controlled LBAM based on infrared image sensing can overcome the effect of the thermal variation and, thus, achieve a consistent processing quality. A three-dimensional finite element model is developed successfully using ANSYS to study the thermal behavior of the molten pool in a building single-bead wall via a closed-loop controlled LBAM process. The temperature distribution, geometrical feature of the molten pool, and cooling rate in different process conditions are investigated. The results from the finite element thermal analysis provide a guidance for the process parameter selection in LBAM, and develop a base for further residual stress analysis.

Acknowledgements

This work was financially supported by THECB, Grants 003613-0022-1999, 003613-0016-2001, NSF, Grants No. DM1-9732848 and DM1-9809198, and the US Department of Education, Grant No. P200A80806-98. Assistance by Dr. H. Mei and Mr. M. Valant during experiments are gratefully acknowledged.

References

[1] R. Kovacevic. Rapid Manufacturing of Functional Parts Based on Deposition by Welding and 3D Laser Cladding. In: Proceedings of the Mold Making 2001 Conference, August 3rd–5th, 2001, Rosemont, IL, by Mold Making Technology Magazine, pp. 263–276.

[2] J.D. Spencer, P.M. Dickens, C.M. Wykes, Rapid prototyping of metal parts by three-dimensional welding. Proceedings of the Institution of Mechanical Engineers. Part B, Journal of Engineering Manufacture 212 (B3) (1998) 175–182.

[3] F. Ribeiro, J. Norrish, R.S. McMaster. Practical Case of Rapid Prototyping Using Gas Metal Arc Welding. In: Proceeding of Conference on Computer Technology in Welding, Paris, 1994, Paper 55.

[4] R.H. Rangel, X. Bian. Metal-Droplet Deformation and Solidification Model with Substrate Remelting. In: Proceedings of the 1996 ASME International Mechanical Engineering Congress and Exposition, Atlanta, Vol. 336, 1996, pp. 265–273.

[5] S. Das, T.P. Fuesting, G. Danyo, L.E. Brown, J.J. Beaman, D.L.

Bourell, K. Sargent. Direct Laser Fabrication of Gas Turbine Engine Component-Microstructure and Properties. In: Solid Freeform Fabrication Proceedings, Austin, 1998, pp. 1–18.

[6] M.L. Griffith, D.M. Keicher, C.L. Atwood, J.A. Romero, J.E. Smugeresky, L.D. Harwell, D.L. Greene. Free Form Fabrication of Metallic Components Using Laser Engineered Net Shaping (LENS). In: Solid Freeform Fabrication Proceedings, Austin, 1996, pp. 125–131.

[7] G.R. Link, J. Fessler, A. Nickel, F. Prinz, Rapid tooling die case inserts using shape deposition manufacturing, Materials and Manufacturing Processes 13 (2) (1998) 263–274.

[8] J.O. Milewski, G.K. Lewis, D.J. Thoma, G.I. Keel, R.B. Nemec, R.A. Reinert, Directed light fabrication of a solid metal hemisphere using 5-axis powder deposition, Journal of Materials Processing Technology 75 (1-3) (1998) 165–172.

[9] D. Hu, H. Mei, R. Kovacevic. Improving solid freeform fabrication by laser based additive manufacturing. Proceedings Institution of Mechanical Engineers, Part B. Journal of Engineering Manufacture (2002) Accepted.

[10] D. Hu, H. Mei, R. Kovacevic. Closed Loop Control of 3D Laser Cladding Based on Infrared Sensing. In: Solid Freeform Fabrication Proceedings, Austin, TX, 2001, pp. 129–137.

[11] I. Kmecko, D. Hu, R. Kovacevic. Controlling Heat Input, Spatter and Weld Penetration in GMA Welding for Solid Freeform Fabrication. In: Solid Freeform Fabrication Proceedings, Austin, TX, 1999, pp. 735–742.

[12] Y.A. Song, S. Park, H. Jee, D. Choi, B. Shin. 3D Welding and Milling—A Direct Approach for Fabrication of Injection Molds. In: Solid Freeform Fabrication Proceedings, Austin, TX, 1999, pp. 793–800.

[13] P.A. Verret, Th. Engel, J. Fontaine, Laser cladding: the relevant parameters for process control, SPIE 2207 (1998) 452–462.

[14] I. Li, W.M. Steen. Sensing, modeling and Closed Loop Control of Powder Feeder for Laser Surface Modification. In: Proceedings of ICALEO, 1993, pp. 965–974.

[15] B. Grunenwald, St. Nowotny, W. Henning, F. Dausinger, H. Hugel. New Technology Developments in Laser Cladding. In: Proceedings of ICALEO, 1993, pp. 934–944.

[16] J.-Y. Jeng, B. Quayle, P.J. Modern, W.M. Steen. Computer Control of Laser Multi-Powder Feeder Cladding System for Optimal Alloy Scan of Corrosion and Wear Resistance. In: Proceedings of LAMP'92, 1992, pp. 819–824.

[17] P.A. Vetter, Th Engel, J. Fontaine, Laser cladding: the relevant parameters for process control, SPIE 2207 (1994) 452–462.

[18] F. Meriaudeau, F. Truchetet, C. Dumont, E. Renier, P. Bolland. Acquisition and Image Processing System Able to Optimize Laser Cladding Process. In: Proceedings of ICSP'96, 1996, pp. 1628–1631.

[19] G.W. Romer, M. Hoeksma, J. Meijer, Industrial imaging controls laser surface treatment, Photonics Spectra 31 (11) (1997) 104–109.

[20] D. Hu, M. Labudovic, R. Kovacevic. On line Sensing of Laser Surface Modification Process by Computer Vision. In: Proceedings of AWS 9th International Conference on Computer Technology in Welding, 1999, pp. 417–424.

[21] W.H. Hofmeister, D.O. MacCallum, G.A. Knorovsky. Video monitoring and control of the LENS process. In: Proceedings of AWS 9th International Conference on Computer Technology in Welding, 1998, pp. 187–196.

[22] J. Mazumder, D. Dutta, N. Kikuchi, A. Ghosh, Closed loop direct metal deposition: art to part, Optics and Laser Engineering 34 (2000) 397–414.

[23] J. Mackerle, Finite element analysis and simulation of welding: a Bibliography (1976–1996), Modelling and Simulation in Materials Science and Engineering 4 (5) (1996) 501–524.

[24] M. Shiomi, A. Yoshidome, F. Abe, K. Osakada, Finite element analysis of melting and solidifying processes in laser rapid prototyping of metallic powders, International Journal of Machine Tools and Manufacture 39 (1999) 237–252.

[25] J. Kim, Y. Peng, Melt pool shape and dilution of laser cladding with wire feeding, Journal of Materials Processing Technology 104 (3) (2000) 284–293.

[26] M. Picasso, A.F.A. Hoadley, Finite element simulation of laser surface treatments including convection in the melt pool, International Journal of Numerical Methods for Heat and Fluid Flow 4 (1) (1994) 61–83.

[27] A. Vasinonta, J.L. Beuth, M. Griffith, A process map for consistent build conditions in the solid freeform fabrication of thin-walled structures, Journal of Manufacturing Science and Engineering 123 (November) (2002) 615–623.

[28] A. Vasinonta, J. L. Beuth, R. Ong, R. Melt Pool Size control in Thin-Walled and Bulky Parts via Process Maps. Solid Freeform Fabrication Proceedings, Austin, TX, 2001, pp. 432–440.